MATERIALS SCIENCE

Giant positive magnetoresistance in half-metallic double-perovskite Sr_2CrWO_6 thin films

Ji Zhang, Wei-Jing Ji, Jie Xu, Xiao-Yu Geng, Jian Zhou,* Zheng-Bin Gu, Shu-Hua Yao, Shan-Tao Zhang*

Magnetoresistance (MR) is the magnetic field–induced change of electrical resistance. The MR effect not only has wide applications in hard drivers and sensors but also is a long-standing scientific issue for complex interactions. Ferromagnetic/ferrimagnetic oxides generally show negative MR due to the magnetic field–induced spin order. We report the unusually giant positive MR up to 17,200% (at 2 K and 7 T) in 12-nm Sr_2CrWO_6 thin films, which show metallic behavior with high carrier density of up to 2.26×10^{28} m^{-3} and high mobility of 5.66×10^4 cm^2 V^{-1} s^{-1}. The possible mechanism is that the external magnetic field suppresses the long-range antiferromagnetic order to form short-range antiferromagnetic fluctuations, which enhance electronic scattering and lead to the giant positive MR. The high mobility may also have contributions to the positive MR. These results not only experimentally confirm that the giant positive MR can be realized in oxides but also open up new opportunities for developing and understanding the giant positive MR in oxides.

INTRODUCTION

The magnetoresistance (MR) effect of a material is the change in electrical resistance in response to an external magnetic field. Materials with large MR are a long-standing goal for research and still at the forefront of contemporary science because of their applications in sensors, memories, and spintronic devices and the fundamental physics of complex interactions. MR is generally defined as $[\rho(H) - \rho(0)]/\rho(0) \times 100\%$, where $\rho(H)$ and $\rho(0)$ are the resistivities with and without magnetic field, respectively. Accordingly, MR can be positive and negative. In general, positive MR occurs in normal metals because of the Lorentz force, but the magnitude is only about a few percent. Giant positive MR has been found in many types of materials, such as magnetic semiconductors (*1*, *2*), small-gap or zero-gap semiconductors (*3*, *4*), ferromagnetic alloys (*5*), topological insulators (*6*), and semimetals (*7*, *8*). Many topological Dirac or Weyl semimetals also show extremely larger positive MR (*9*–*13*). Negative MR, on the other hand, specifically relates to the multilayer structure of adjacent ferromagnetic layers (metals or ABO_3-type perovskite oxides), known as giant MR (GMR) and colossal MR (CMR). In the GMR and CMR materials, the magnetic field reduces the local spin disorder and thus decreases resistivity and leads to negative GMR or CMR (*14*–*18*).

Ferromagnetic ABO_3-type perovskite oxide generally illustrates negative CMR (*15*–*19*), although, by artificial microstructure design, positive MR can be achieved in perovskite oxides, but the MR value is very small (*20*, *21*). ABO_3-type perovskite oxides provide structural flexibility to tune functional properties. For example, by introducing B and B′ to the B site alternatively, that is, forming B site–ordered $A_2BB'O_6$-type double-perovskite ferrimagnetic oxides, which generally show extremely high Curie temperatures (*17*, *22*), positive MR with a moderate value of up to ~265% can be achieved (*23*–*27*). However, at least two issues about the positive MR in double-perovskite ferrimagnetic oxides need further investigations. The first issue is that the reported phenomenon is delicately dependent on experimental parameters. In most cases, double-perovskite materials show negative MR (*17*, *28*), and only a few studies report the positive MR (*23*–*27*) or even both the positive and negative MR (*29*, *30*). These paradoxical phenomena are due to the existence and domination of long-range magnetic field–induced ferromagnetic background (*15*, *31*), which tends to result in negative MR (*14*–*18*). The other issue is that all the experimentally observed positive MRs in double-perovskite oxides (*23*–*27*, *29*, *30*) are about three to four orders of magnitude lower than those in semimetals or semiconductors (*1*–*13*). Therefore, ferromagnetic/ferromagnetic oxides with giant positive MRs are still desirable.

Here, we report the robust giant positive MR up to 17,200% (at 2 K and 7 T) in half-metallic double-perovskite Sr_2CrWO_6 (SCWO) thin films fabricated under low pressure and discuss the mechanism of the GMR. SCWO is a typical $A_2BB'O_6$-type double-perovskite oxide, where Cr^{3+} and W^{5+} occupy the B and B′ sites, alternatively. The antiferromagnetic coupling between Cr^{3+} ($3d^3$, $S = 3/2$) and W^{5+} ($5d^1$, $S = 1/2$) leads to a macroscopic ferrimagnetic nature with a net magnetization of 2 μ_B/formula unit (f.u.), as will be shown in the following theoretical calculation. The corresponding Curie temperature (T_c) is ~460 K (*28*, *32*). However, the synthesis of single-phase, high-quality SCWO is very difficult due to the parasitic phases (*33*, *34*). Therefore, only several experimental works on SCWO have been reported (*30*, *32*–*34*).

RESULTS

Figure 1 (A to C) shows the atomic force microscopy (AFM) surface morphologies of the SCWO films deposited for 1000, 2000, and 4000 laser pulses under a low pressure of 10^{-5} Pa. As can be seen, all films show very flat surfaces, and the surface roughness increases slightly as the thickness increases, indicating the high quality of these films. The root mean square surface roughness is 348.4, 502.7, and 1420 pm for the three films, respectively. From the typical cross-sectional transmission electron microscopy (TEM) morphology of the films deposited for 4000 pulses shown in Fig. 1D, the thicknesses of the films deposited for 1000, 2000, and 4000 pulses are 12, 24, and 48 nm, respectively, which are abbreviated as S-1, S-2, and S-3, respectively. The homogeneous cross-sectional TEM morphology and the sharp, coherent substrate-film interface (Fig. 1, D to F) indicate the high quality of the epitaxial films, which is further confirmed by the x-ray diffraction (XRD) measurements (fig. S1). Both S-1 and S-2 only show diffraction

National Laboratory of Solid State Microstructures and Department of Materials Science and Engineering, College of Engineering and Applied Science and Collaborative Innovation Center of Advanced Microstructures, Nanjing University, Nanjing 210093, China.
*Corresponding author. Email: zhoujian@nju.edu.cn (J.Z.); stzhang@nju.edu.cn (S.-T.Z.)

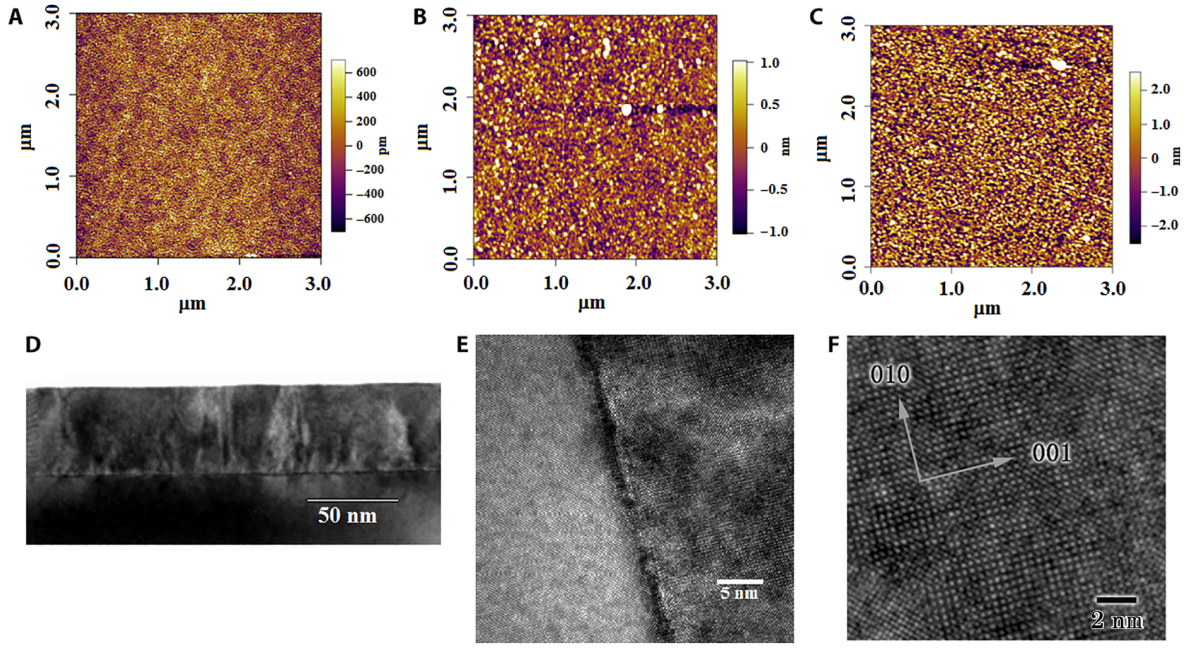

Fig. 1. The AFM and TEM morphologies of the SCWO films. (**A**) S-1 (12 nm thick). (**B**) S-2 (24 nm thick). (**C**) S-3 (48 nm thick). The surface roughness increases with film thickness with values of 348.4 pm, 502.7 pm, and 1.42 nm, respectively. (**D**) Cross-sectional TEM morphology of the S-3 films. (**E** and **F**) The homogeneous thin films, sharp substrate-film interface, and high-resolution TEM indicate the high quality of the films.

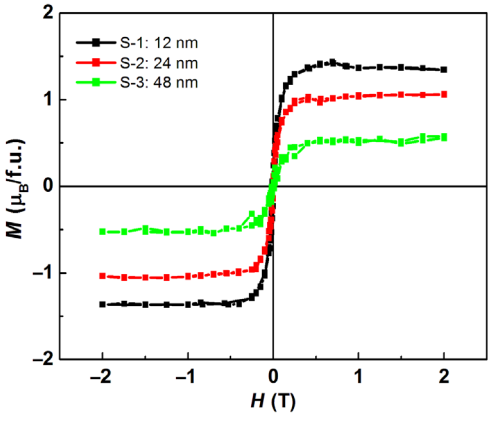

Fig. 2. Magnetization-magnetic field (*M-H*) curves of the S-1, S-2 and S-3 SCWO films. All films show well-saturated *M-H* loops, indicating the ferromagnetic nature.

shoulders at the left of the $SrTiO_3$ (STO) diffraction peaks, indicating that the films are well strained to form a coherent interface with the (001) STO substrate surface. By noting that STO has a cubic structure with a lattice constant of a = 3.90 Å and that SCWO has a cubic structure with a lattice constant of a = 7.89 Å (*30*), it is deduced that S-1 and S-2 should have a slight compressive strain. With increasing thickness, the strain tends to relax. Therefore, S-3 has an obvious independent diffraction peak.

The magnetization-magnetic field (*M-H*) curves of all the samples under low pressure were measured at 10 K with a magnetic field of 2 T and plotted in Fig. 2. The maximum magnetization values are 1.4, 1.1, and 0.6 μ_B/f.u. for the S-1, S-2, and S-3 thin films, respectively, which are smaller than the theoretical prediction of 2.0 μ_B/f.u., as will be shown later. The decreasing magnetization in the double perovskite is usually due to the anti-site defects (ASDs) or the oxygen vacancy (*28*, *35*). However, we believe that the concentration of ASD or the oxygen vacancy should not be very high because we find that the films have a very small resistivity, as we will discuss later. The magnetization values obtained here are closer to those reported by other studies on SCWO films (*30*, *34*), and the magnetization increases monotonically as the temperature decreases in the temperature range between 10 and 300 K (fig. S2), which is attributed to the ferrimagnetic nature of SCWO (*30*, *32*).

The temperature dependence of the resistivity (ρ) was measured by method-1 (schematically shown in fig. S3A) with and without an external magnetic field (2 T), which is shown in Fig. 3 (A to C). Without magnetic field, all films show a metallic behavior in the whole temperature range (that is, the resistivity increases as the temperature increases). The measured resistivities at 2 and 300 K are 4.9×10^{-11} and 9.5×10^{-7} ohm·m, 4.5×10^{-10} and 1.1×10^{-6} ohm·m, and 9.2×10^{-10} and 3.7×10^{-6} ohm·m for the S-1, S-2, and S-3 thin films, respectively. The resistivity of the SCWO thin films is comparable to that of a good metal and much smaller than that reported by others on SCWO epitaxial films or bulk ceramics (*30*, *32*–*34*). The residual resistance ratios (RRR) between 300 and 2 K are 19,387, 2444, and 4111 for the S-1, S-2, and S-3 thin films, respectively. The extremely high RRR value again confirms the good quality of these films. To extract the characteristics of the carriers and carrier density, we measured the temperature-dependent Hall effect. The corresponding calculated temperature-dependent carrier density and mobility of all samples are plotted in Fig. 4 (A and B), respectively (the inset of Fig. 4B presents the Hall coefficient). At 2 K, the n-type carrier densities were calculated to be 2.25×10^{28} m^{-3}, 1.18×10^{28} m^{-3}, and 3.82×10^{27} m^{-3} for the S-1, S-2, and S-3 thin films, respectively. The carrier density shows almost negligible temperature dependence. The mobilities, on the other hand, were 5.66×10^4, 1.18×10^4, and 1.78×10^4 cm^2 V^{-1} s^{-1} for the S-1, S-2, and S-3 thin films, respectively, at 2 K. For each film, the mobility decreases as the temperature increases.

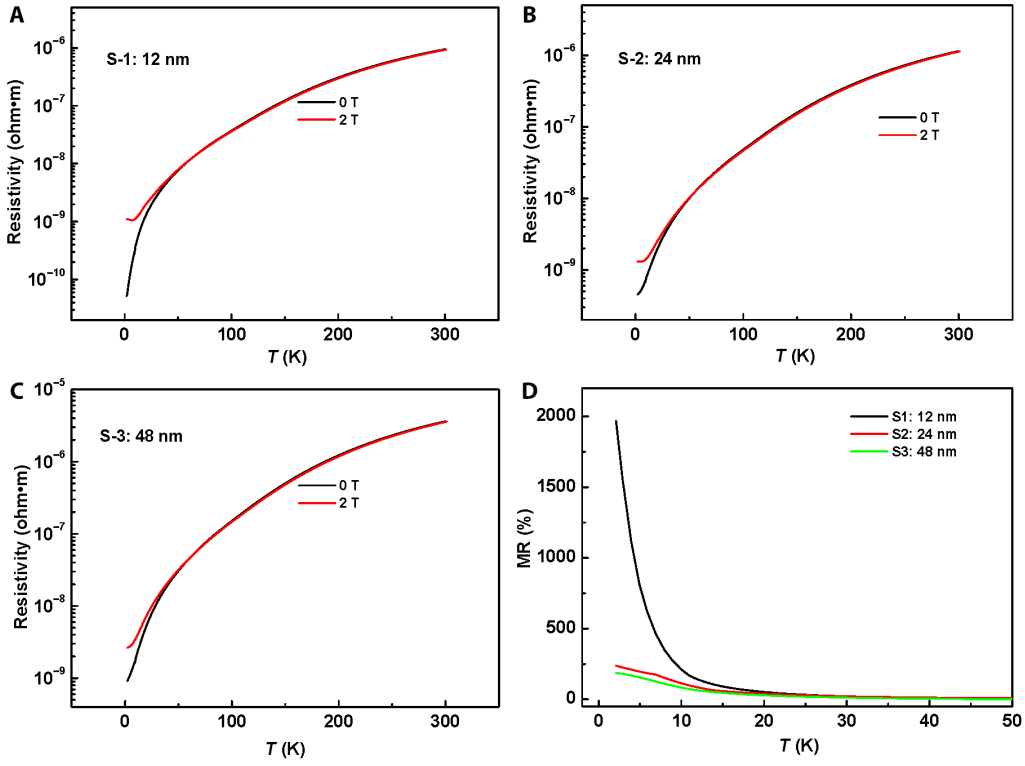

Fig. 3. Temperature-dependent resistivity (ρ-*T*) and temperature-dependent MR of the SCWO films. ρ-*T* of (**A**) S-1, (**B**) S-2, and (**C**) S-3 without and with a magnetic field of 2 T. Without magnetic field, all films show metallic behavior indicated by the decreasing resistivity with decreasing field in the whole temperature range. When an applied magnetic field perpendicular to the thin film is applied, the resistivity tends to increase with decreasing field at the low temperature range. (**D**) MR-*T* of all the films. At 2 K with a magnetic field of 2 T, the positive MRs are 1960, 245, and 190% for the films, respectively.

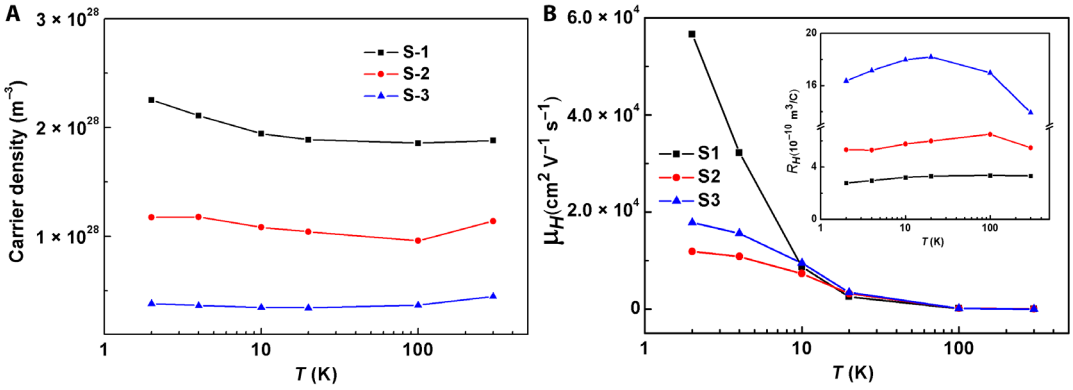

Fig. 4. Temperature-dependent carrier density and mobility of the SCWO films. The films show very high carrier density and high mobility at low temperature; the inset depicts Hall coefficient.

It is necessary to emphasize that low pressure during deposition is important to obtain high-quality samples. As a comparison, two SCWO films were also deposited on the (001) STO substrate for 2000 pulses under oxygen pressures of 0.5 and 1.5 Pa. Although the XRD patterns indicate that the films are well oriented along the *c*-axis (fig. S4), the AFM and TEM morphologies show that the films deposited under relatively higher oxygen pressures have rougher surfaces (fig. S5). The temperature-dependent resistance of the SCWO films fabricated under an oxygen pressure of 0.5 Pa is plotted in fig. S6. The figure shows a semiconductor-like behavior in the whole temperature range, which is due to the bad quality of the film. The SCWO films fabricated under an oxygen pressure of 1.5 Pa show similar behavior in the higher temperature range, but the resistance is too high to be measured in the lower temperature range. Here, we will focus on the films fabricated under low oxygen pressure (10^{-5} Pa).

However, the low pressure during sample fabrication could induce the oxygen vacancies in both the SCWO films and the STO substrate. The oxygen vacancies have different effects on the SCWO films and the STO substrate. For the metallic SCWO films, they can increase the scattering of the electrons and the resistivity of the materials, which can even possibly lead to the semiconductor behavior due to the defective band that crosses the Fermi level (*36*–*42*). However, as shown

above, the resistivity of the three films is very small, which is comparable to that of the best metals. Therefore, we believe that the oxygen vacancy has no predominant effect on the transport property in these thin films.

The oxygen vacancies, on the other hand, have a totally different effect on the insulating STO substrate. The oxygen vacancies can introduce carriers in the insulator or semiconductor and increase the electric conductivities. It is well known that the oxygen-deficient STO behaves like metals (*43*, *44*). Therefore, it is interesting to know the impact of the low pressure–induced oxygen vacancies on the STO substrate and how the oxygen vacancies affect the transport and MR results. To investigate these influences, the bare STO substrate was heated at the same temperature (830°C) and pressure (10^{-5} Pa), and then the temperature-dependent resistance was measured as shown in fig. S3. The resistance was first measured by method-1, which is schematically shown in fig. S3A, and the result is shown in fig. S3B. It is found that the heated bare STO substrate shows metallic behavior due to the oxygen vacancies, which is consistent with other reports (*34*, *43*, *44*). However, two important features should be emphasized. The first feature is that the resistance of the heated bare STO is at least two orders of magnitude higher than that of the SCWO film (S-2) that is measured with the same method. With a simple model, the resistances of the STO substrate and the SCWO film are in parallel connection; therefore, the significantly smaller resistance of the SCWO film should be dominant for the macroscopic resistance (that is, the resistance of the STO can be neglected). The second feature is that the heated bare STO shows almost zero MR in the whole temperature range (fig. S3C), consistent with a previous report (*44*). Because our SCWO films show the giant positive MR at low temperatures (fig. S3D and Fig. 3), as will be discussed later, the heated STO has almost no influence on the macroscopic MR. For further confirmation, the resistivity and MR of the S-2 films with the same geometry size were measured by using the wire bonding techniques, as schematically shown in fig. S3A (labeled as method-2); the result is shown in fig. S3D. In this case, the contributions of both the substrate and the film to macroscopic transport properties are measured together. As can be seen from fig. S3 (B and D), good metallic behavior and giant positive MR are still observable. The results are similar to those measured in the SCWO films but different from those in the heated bare STO substrate. On the basis of these discussions, it may be reasonable to conclude that the contribution from oxygen vacancy of the heated STO substrates to the macroscopic transport property and MR should be negligible.

Here, it is also necessary to briefly discuss the effect of strain on magnetic property. In general, strain in ultrathin metallic perovskite oxide films can induce metal-insulator transition; the critical thickness is less than 10 units (for example, <4.0 nm) (*41*, *45*). However, the thicknesses of our films are 12, 24, and 48 nm, indicating that these SCWO films are quasi–two-dimensional or even three-dimensional, that is, the strain cannot have determinant contributions to the transport nature of these films.

To understand the basic physical properties of SCWO, we have calculated its band structure and density of states (DOS) by the OpenMX code (*46*) within the framework of the density functional theory in the generalized gradient approximation (*47*). From the results shown in Fig. 5, we can see that SCWO is a perfect half-metal, where one spin component shows the metallic properties and the other has a large band gap of about 2.3 eV. The half-metallicity nature of SCWO is commonly found in double-perovskite materials, such as Sr_2FeMoO_6 (*17*). Note that the SCWO is definitely not a semimetal or

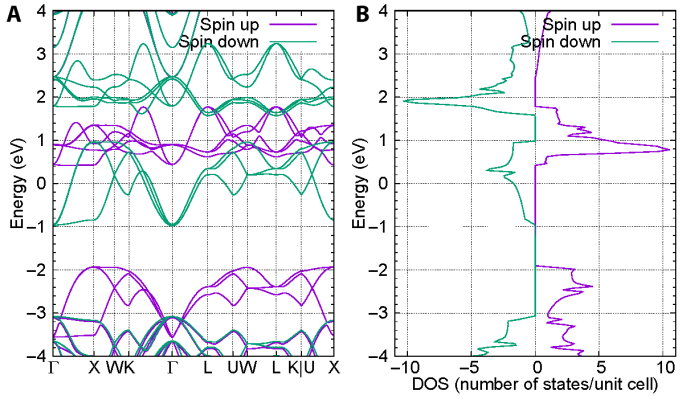

Fig. 5. Theoretical calculated electronic properties of SCWO. (**A**) The spin-polarized band structure and (**B**) DOS of SCWO. Fermi energy is set to 0. The SCWO is a perfect half-metal with the total net spin moment is 2.0 μ_B/f.u.

a zero-gap semiconductor from the band structure. Besides, we find that the total net spin moment is 2.0 μ_B/f.u. in our calculation, which is the same as the theoretical expectation. Because of the ASD or oxygen vacancies in SCWO, the observed magnetization in our experiments is smaller than that of calculated results mentioned above.

As shown in Fig. 3 (A to D), when an external 2-T magnetic field perpendicular to the thin film is applied, the resistivity of each sample tends to increase when the temperature is lower than 20 K and increases sharply when the temperature is lower than 10 K. This increased resistivity leads to a giant positive MR of 1960%, 245%, and 190% at 2 K for SCWO films S-1, S-2, and S-3, respectively. It is found that the positive MR has negligible dependence on the external magnetic field direction. As evidenced by the temperature-dependent resistivity of S-2 between 2 and 300 K with the applied magnetic field parallel to the thin film (but still perpendicular to the electric current) (fig. S7), the positive MR value is about 235% at 2 K, which is very close to that in Fig. 3B.

Figure 6 shows the field-dependent MR of the S-1, S-2, and S-3 thin films at 2, 4, 10, and 20 K. The maximum positive MR values at 2 K and 7 T are 17,200%, 2060%, and 1185% for S-1, S-2, and S-3, respectively. The MR shows no saturation trace even up to 14 T, as confirmed by the field-dependent MR of the S-2 films (fig. S8). To the best of our knowledge, this positive MR is the largest value ever observed in ferromagnetic/ferrimagnetic perovskite oxides and is two orders larger than that reported by others on half-metallic double-perovskite oxide thin films or bulks (*23*–*27*, *29*, *30*).

DISCUSSION

We will first analyze the mechanism of the giant positive MR in SCWO thin films. In our opinion, the mechanism for the giant positive MR here might be a very novel one. We therefore can only provide the following discussion. Recently, it is theoretically proposed that giant positive MR could be observed in the antiferromagnetic metallic double perovskite (*31*). An applied field could suppress the long-range antiferromagnetic ordering, leading to a state with short-range antiferromagnetic correlations and strong electronic scattering, which induces the giant positive MR. According to the above discussion, our SCWO thin films show very good quality and metallicity, which implies a long-range antiferromagnetic ordering (ferrimagnetic) and high spin ordering degree. Therefore, the SCWO could possibly be a materialization of the

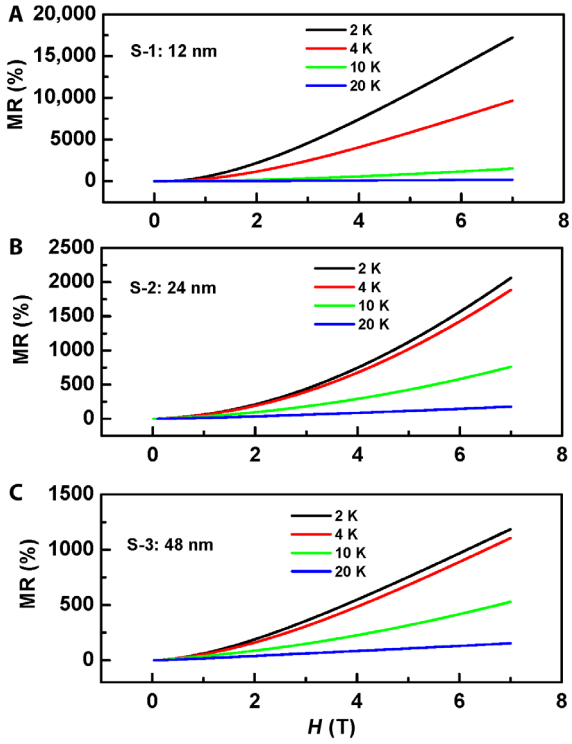

Fig. 6. Magnetic field–dependent positive MR at 2, 4, 10, and 20 K for the SCWO films. (**A**) S-1. (**B**) S-2. (**C**) S-3. Giant positive MR with values of 17,200, 2060, and 1185%, respectively, can be observed at 2 K with a magnetic field of 7 T.

theoretical model (*31*). When an external magnetic field is applied, the long-range antiferromagnetic ordering will be suppressed, as schematically shown in fig. S9. Therefore, there will be short-range, correlated antiferromagnetic fluctuations embedded in the field-induced ferromagnetic background, that is, numerous localized spin disordering patches with different orientations are formed. These patches can significantly enhance the electronic scattering, leading to the observed giant positive MR. It is emphasized that such a field-induced spin disorder concept is in contrast to the conventional ferromagnetic materials, where the field induces high spin ordering (*16*).

It is noted from Fig. 3 that without the external magnetic field, the resistivity slightly increases as the film thickness increases, which is due to the increased ASD content. As a result, the positive MR decreased as the film thickness and ASD concentration increased, which is also consistent with the theoretical prediction (*31*). Furthermore, according to the theoretical model, the positive MR increases first and then decreases as the magnetic field increases because the high magnetic field can even shift the antiferromagnetic order to the ferromagnetic one, which are both long-range ordering states. However, we have not observed any saturation or decrease of MR of up to 14 T, which is quite possible considering that a magnetic field of 14 T is not sufficiently high.

We cannot exclude, on the other hand, other possible mechanisms for the giant positive MR. As we mentioned in the Introduction, in recent years, many semimetals, such as WTe_2, LaSb, ZrSiS, and WP_2, are found to have an extremely large and nonsaturating positive MR (*8*–*10*, *13*). The possible mechanisms for the high MR in semimetals may be the electron-hole compensation (*10*) or the extremely high electric conductivity and high mobility (*9*, *48*); the latter one does not require the semimetallicity and can be extended to other types of materials. It is obvious that the SCWO is not a semimetal according to Fig. 5, but the carrier mobility is also very high, as shown in Fig. 4B. Therefore, the high mobility in the SCWO thin films could also be the possible origin of the giant and nonsaturating positive MR. Especially, it is observed that when the thickness of the films increases, the conductivity and the mobility decrease because of the increase of ASD, leading to the decrease of MR, which is possibly due to the decrease of the mobility.

However, it seems that we cannot distinguish the above two mechanisms based on the present work; thus, more future experimental works are needed. For these studies, high-quality samples with metallic nature and low ASD might be the key factor because ASD plays a detrimental role in suppressing conductivity and, therefore, mobility (*49*, *50*).

Finally, we need to exclude the possible contributions of nanosized Cr, CrO_2, or Cr_2O_3 clusters, which might be formed during sample fabrication or processing, to macroscopic transport properties. According to literatures, metallic Cr or CrO_2 shows negative MR (*14*, *51*), whereas insulating Cr_2O_3 cannot lead to the observed metallicity and thus large positive MR. Both are in contrast to our experimental results. Therefore, it is reasonable that Cr or CrO_x is not responsible for the observed giant positive MR. Metal Cr is not detectable because the Cr cations have mixed valences of +2 and +3 at room temperature and at a low temperature of 14 K (*52*), as shown in fig. S10A. In addition, the x-ray photoelectron spectroscopy (XPS) measurements confirm that there is no W metal (fig. S10B). The asymmetric peaks centered around 35.4 and 37.6 eV should be the sum of two peaks. According to the simulation, the peaks around 35.0 and 37.2 eV are attributed to W^{5+}, whereas those around 35.7 and 37.8 eV are attributed to W^{6+} (*53*). This means the W cations have mixed valence states of +5 and +6. One of the possible reason for the formation of W^{6+} is that Ar^+ ions sputter on the surface, disrupt the lattice, alter bonding environments, and change the surface stoichiometry progressively, thus leading to locally changed valences of the surface cations (*54*). The other possible reason for the formation of W^{6+} is that the existence of Cr^{2+} maintains charge neutrality. The coexistence of mixed valence states is common in double-perovskite oxides (*18*) and may have little influence on properties. Here, W^{6+} ($5d^0$, $S = 0$) shows no magnetic moment, and its content should be very limited; otherwise, the magnetization should be very weak. For charge neutrality, the content of Cr^{2+} should be limited accordingly. The Cr^{3+} ($3d^3$, $S = 3/2$) and local Cr^{2+} ($3d^4$, $S = 2$) will antiferromagnetically interact with W^{5+} ($5d^1$, $S = 1/2$). Hence, different valence states of W and Cr cations will locally disrupt the antiferromagnetic interaction, leading to locally complex magnetic interaction, but will not break the whole ferrimagnetic nature of SCWO.

In conclusion, unusually giant positive MR up to 17,200% is observed in half-metallic ferrimagnetic SCWO films deposited under low pressure. This finding is possibly attributed to the fact that external magnetic field suppresses the long-range antiferromagnetic coupling between Cr and W cations, leading to short-range spin fluctuations. This field-induced spin disorder enhances the electronic scattering and thus results in positive MR. At the same time, high mobility may also contribute to the giant positive MR. In addition, ASD can suppress the positive MR by forming local antiferromagnetic regions, which destroy the metallic nature of SCWO. We believe that this work not only sets a record for the giant positive MR in magnetic perovskite oxides but also stimulates further investigation and understanding of the MR materials.

MATERIALS AND METHODS

Sample preparation

SCWO thin films were prepared on a (001) STO substrate by pulsed laser deposition using a 248-nm KrF excimer laser. A stoichiometric SCWO ceramic was used as the target. Before each deposition, the chamber was evacuated to a base pressure of 10^{-5} Pa. During each deposition, the substrate temperature was 830°C, the laser repetition rate was 2 Hz, the laser energy density was 1.2 J/cm^2, and the pressure was 10^{-5} Pa. After each deposition, the films were in situ annealed in the chamber for 10 min, cooled to 400°C at a rate of −10°C/min, and then naturally cooled to room temperature.

Structural and property measurements

The structures of the films were investigated by XRD (Rigaku Ultima III), AFM (Cypher), and TEM (FEI Tecnai F20). The cross-sectional sample for TEM was prepared by ion milling with 3.2- to 4.5-keV Ar^+ ions for a few hours after mechanical thinning. The chemical valence states of the Cr and W cations were studied by soft x-ray absorption spectroscopy [BL12B-a, National Synchrotron Radiation Laboratory (NSRL)] and XPS measurements (K-Alpha, Thermo Scientific), respectively. The magnetic and transport properties were measured by using a superconductor quantum interference device (MPMS XL-7, Quantum Design) and a physical property measurement system (PPMS-9 and PPMS-16, Quantum Design).

First-principles calculations

The band structure and DOS of double-perovskite SCWO were calculated by the OpenMX code (*46*) within the framework of the density functional theory in the generalized gradient approximation (*47*). SCWO has a cubic structure with the space group of $Fm\bar{3}m$, and its experimental lattice constant (a = 7.89 Å) was used in our calculation (*34*). The bases used in the OpenMX code were $s^3p^2d^2f^2$, $s^3p^3d^2$, $s^3p^2d^2f^1$, and $s^2p^2d^1$ for Sr, Cr, W, and O elements, respectively. The energy cutoff for real-space integration is 300 rydbergs, and a k-points mesh of 15 × 15 × 15 was used for the Brillouin zone integration. To include the effects of the on-site Coulomb energy U, we used the effective Hubbard U of 2.13 eV for Cr (*55*).

SUPPLEMENTARY MATERIALS

Supplementary material for this article is available at http://advances.sciencemag.org/cgi/content/full/3/11/e1701473/DC1

fig. S1. XRD patterns of the SCWO films with different thicknesses.
fig. S2. Field cooling (200 Oe) temperature-dependent magnetization of the S-1, S-2, and S-3 films.
fig. S3. The methods for transport property measurement and the transport properties of the heated bare STO substrate and S-2 films with and without a magnetic field.
fig. S4. XRD patterns of the SCWO films fabricated with oxygen pressures of 0.5 and 1.5 Pa.
fig. S5. AFM and cross-sectional TEM images of the SCWO films fabricated with an oxygen pressure of 0.5 Pa.
fig. S6. The temperature-dependent resistance of the films deposited under an oxygen pressure of 0.5 Pa.
fig. S7. The temperature-dependent resistivity of the S-2 films with the external magnetic field parallel to the thin film but still perpendicular to the current.
fig. S8. Field-dependent MR of the S-2 films up to 14 T.
fig. S9. Evolution of magnetic structure and magnetic domain of the SCWO without and with a magnetic field.
fig. S10. The valence states of Cr and W cations.

REFERENCES AND NOTES

1. Y. Matsumoto, M. Murakami, T. Shono, T. Hasegawa, T. Fukumura, M. Kawasaki, P. Ahmet, T. Chikyow, S. Koshihara, H. Koinuma, Room-temperature ferromagnetism in transparent transition metal-doped titanium dioxide. *Science* **291**, 854–856 (2001).
2. M. Jamet, A. Barski, T. Devillers, V. Poydenot, R. Dujardin, P. Bayle-Guillemaud, J. Rothman, E. Bellet-Amalric, A. Marty, J. Cibert, R. Mattana, S. Tatarenko, High-Curie-temperature ferromagnetism in self-organized $Ge_{1-x}Mn_x$ nanocolumns. *Nat. Mater.* **5**, 653–659 (2006).
3. R. Xu, A. Husmann, T. F. Rosenbaum, M.-L. Saboungi, J. E. Enderby, P. B. Littlewood, Large magnetoresistance in non-magnetic silver chalcogenides. *Nature* **390**, 57–60 (1997).
4. J. Hu, T. F. Rosenbaum, Classical and quantum routes to linear magnetoresistance. *Nat. Mater.* **7**, 697–700 (2008).
5. N. Manyala, Y. Sidis, J. F. DiTusa, G. Aeppli, D. P. Young, Z. Fisk, Magnetoresistance from quantum interference effects in ferromagnets. *Nature* **404**, 581–584 (2000).
6. X. L. Wang, Y. Di, S. X. Dou, C. Zhang, Room temperature giant and linear magnetoresistance in topological insulator Bi_2Te_3 nanosheets. *Phys. Rev. Lett.* **108**, 266806 (2012).
7. F. Y. Yang, K. Liu, K. Hong, D. H. Reich, P. C. Searson, C. L. Chien, Large magnetoresistance of electrodeposited single-crystal bismuth thin films. *Science* **284**, 1335–1337 (1999).
8. L.-K. Zeng, R. Lou, D.-S. Wu, Q. N. Xu, P.-J. Guo, L.-Y. Kong, Y.-G. Zhong, J.-Z. Ma, B.-B. Fu, P. Richard, P. Wang, G. T. Liu, L. Lu, Y.-B. Huang, C. Fang, S.-S. Sun, Q. Wang, L. Wang, Y.-G. Shi, H. M. Weng, H.-C. Lei, K. Liu, S.-C. Wang, T. Qian, J.-L. Luo, H. Ding, Compensated semimetal LaSb with unsaturated magnetoresistance. *Phys. Rev. Lett.* **117**, 127204 (2016).
9. M. N. Ali, L. M. Schoop, C. Garg, J. M. Lippmann, E. Lara, B. Lotsch, S. S. P. Parkin, Butterfly magnetoresistance, quasi-2D Dirac Fermi surface and topological phase transition in ZrSiS. *Sci. Adv.* **2**, e1601742 (2016).
10. M. N. Ali, J. Xiong, S. Flynn, J. Tao, Q. D. Gibson, L. M. Schoop, T. Liang, N. Haldolaarachchige, M. Hirschberger, N. P. Ong, R. J. Cava, Large, non-saturating magnetoresistance in WTe_2. *Nature* **514**, 205–208 (2014).
11. L. P. He, X. C. Hong, J. K. Dong, J. Pan, Z. Zhang, J. Zhang, S. Y. Li, Quantum transport evidence for the three-dimensional Dirac semimetal phase in Cd_3As_2. *Phys. Rev. Lett.* **113**, 246402 (2014).
12. W. Gao, N. Hao, F.-W. Zheng, W. Ning, M. Wu, X. Zhu, G. Zheng, J. Zhang, J. Lu, H. Zhang, C. Xi, J. Yang, H. Du, P. Zhang, Y. Zhang, M. Tian, Extremely large magnetoresistance in a topological semimetal candidate pyrite $PtBi_2$. *Phys. Rev. Lett.* **118**, 256601 (2017).
13. N. Kumar, Y. Sun, N. Xu, K. Manna, M. Yao, V. Süss, I. Leermakers, O. Young, T. Förster, M. Schmidt, B. Yan, U. Zeitler, M. Shi, C. Felser, C. Shekhar, Extremely high magnetoresistance and conductivity in the type-II Weyl semimetal WP_2 and MoP_2. https://arxiv.org/abs/1703.04527 (*2017*).
14. M. N. Baibich, J. M. Broto, A. Fert, F. Nguyen van Dau, F. Petroff, P. Etienne, G. Creuzet, A. Friederich, J. Chazelas, Giant magnetoresistance of (001)Fe/(001)Cr magnetic superlattices. *Phys. Rev. Lett.* **61**, 2472–2475 (1988).
15. A. Fert, Origin, development, and future of spintronics (Nobel Lecture). *Angew. Chem. Int. Ed.* **47**, 5956–5969 (2008).
16. M. B. Salamon, M. Jaime, The physics of manganites: Structure and transport. *Rev. Mod. Phys.* **73**, 583–628 (2001).
17. K.-I. Kobayashi, T. Kimura, H. Sawada, K. Terakura, Y. Tokura, Room-temperature magnetoresistance in an oxide material with an ordered double-perovskite structure. *Nature* **395**, 677–680 (1998).
18. W.-t. Chen, M. Mizumaki, H. Seki, M. S. Senn, T. Saito, D. Kan, J. P. Attfield, Y. Shimakawa, A half-metal A- and B-site-ordered quadruple perovskite oxide $CaCu_3Fe_2Re_2O_{12}$ with large magnetization and a high transition temperature. *Nat. Commun.* **5**, 3909 (2014).
19. J. Lloyd-Hughes, C. D. W. Mosley, S. P. P. Jones, M. R. Lees, A. Chen, Q. X. Jia, E.-M. Choi, J. L. MacManus-Driscoll, Colossal terahertz magnetoresistance at room temperature in epitaxial $La_{0.7}Sr_{0.3}MnO_3$ nanocomposites and single-phase thin films. *Nano Lett.* **17**, 2506–2511 (2017).
20. K. Zhao, M. He, H.-b. Lu, Low-field positive magnetoresistance near room temperature in three-component perovskite-type artificial superlattices. *Appl. Phys. Lett.* **91**, 152507 (2007).
21. K.-j. Jin, H.-b. Lu, K. Zhao, C. Ge, M. He, G.-z. Yang, Novel multifunctional properties induced by interface effects in perovskite oxide heterostructures. *Adv. Mater.* **21**, 4636–4640 (2009).
22. H. L. Feng, M. Arai, Y. Matsushita, Y. Tsujimoto, Y. Guo, C. I. Sathish, X. Wang, Y.-H. Yuan, M. Tanaka, K. Yamayra, High-temperature ferrimagnetism driven by lattice distortion in double perovskite Ca_2FeOsO_6. *J. Am. Chem. Soc.* **136**, 3326–3329 (2014).
23. K.-W. Kim, S. Ghosh, S. Buvaev, S. Mhin, J. L. Jones, A. F. Hebard, D. P. Norton, Magnetic and magnetotransport properties of Ba_2FeMoO_6 pulsed laser deposited thin films. *J. Appl. Phys.* **112**, 083923 (2012).
24. M.-R. Li, M. Retuerto, Z. Deng, P. W. Stephens, M. Croft, Q. Huang, H. Wu, X. Deng, G. Kotliar, J. Sánchez-Benítez, J. Hadermann, D. Walker, M. Greenblatt, Giant magnetoresistance in the half-metallic double-perovskite ferrimagnet Mn_2FeReO_6. *Angew. Chem. Int. Ed.* **54**, 12069–12073 (2015).
25. A. M. Arévalo-López, G. M. McNally, J. P. Attfield, Large magnetization and frustration switching of magnetoresistance in the double-perovskite ferrimagnet Mn_2FeReO_6. *Angew. Chem. Int. Ed.* **54**, 12074–12077 (2015).

26. G. Popov, M. Greenblatt, M. Croft, Large effects of *A*-site average cation size on the properties of the double perovskite $Ba_{2-x}Sr_xMnReO_6$: A d^5-d^1 system. *Phys. Rev. B* **67**, 024406 (2003).
27. L. S. Lobanovskii, I. O. Troyanchuk, N. V. Pushkarev, G. Szymczak, Magnetoresistance effect in $A_2(FeMo)O_x$ double perovskite (A = Sr, Ca; $5.90 \leq x \leq 6.05$). *Phys. Solid State* **43**, 677–681 (2001).
28. D. Serrate, J. M. De Teresa, M. R. Ibarra, Double perovskites with ferromagnetism above room temperature. *J. Phys. Condens. Matter* **19**, 023201 (2007).
29. H. Asano, S. B. Ogale, J. Garrison, A. Orozco, Y. H. Li, E. Li, V. Smolyaninova, C. Galley, M. Downes, M. Rajeswari, R. Ramesh, T. Venkatesan, Pulsed-laser-deposited epitaxial Sr_2FeMoO_{6-y} thin films: Positive and negative magnetoresistance regimes. *Appl. Phys. Lett.* **74**, 3696–3698 (1999).
30. J. B. Philipp, D. Reisinger, M. Schonecke, A. Marx, A. Erb, L. Alff, R. Gross, J. Klein, Spin-dependent transport in the double-perovskite Sr_2CrWO_6. *Appl. Phys. Lett.* **79**, 3654–3656 (2001).
31. V. N. Singh, P. Majumdar, Huge positive magnetoresistance in antiferromagnetic double perovskite metals. *J. Phys. Condens. Matter* **26**, 296001 (2014).
32. J. B. Philipp, P. Majewski, L. Alff, E. Erb, R. Gross, T. Graf, M. S. Brandt, J. Simon, T. Walther, W. Mader, D. Topwal, D. D. Sarma, Structural and doping effects in the half-metallic double perovskite A_2CrWO_6 (A = Sr, Ba, Ca). *Phys. Rev. B* **68**, 144431 (2003).
33. B. Fisher, K. B. Chashka, L. Patlagan, G. M. Reisner, Bulk properties, intergrain zero-field conductivity, *I–V* characteristics and magnetotransport of $Sr_2Cr_{1+x}W_{1-x}O_6$ (x = 0, 1/3). *Phys. Rev. B* **71**, 104428 (2005).
34. J. B. Phillipp, D. Reisinger, M. Schonecke, M. Opel, A. Marx, A. Erb, L. Alff, R. Gross, Epitaxial growth and transport properties of Sr_2CrWO_6 thin films. *J. Appl. Phys.* **93**, 6853–6855 (2003).
35. L. Balcells, J. Navarro, M. Bibes, A. Roig, B. Martínez, J. Fontcuberta, Cationic ordering controlling of magnetization in Sr_2FeMoO_6 double perovskite. *Appl. Phys. Lett.* **78**, 781–783 (2001).
36. C. Ma, M. Liu, G. Collins, H. Wang, S. Bao, X. Xu, E. Enriquez, C. Chen, Magnetic and electric transport properties of $LaBaCo_2O_{5.5+\delta}$ thin films on vicinal (001) $SrTiO_3$ surfaces. *ACS Appl. Mater. Interfaces* **5**, 451–455 (2013).
37. Q. Wang, A. Puntambekar, V. Chakrapani, Vacancy-induced semiconductor–insulator–metal transitions in nonstoichiometric nickel and tungsten oxides. *Nano Lett.* **16**, 7067–7077 (2016).
38. Z. Harrell, E. Enriquez, A. Chen, P. Dowden, B. Mace, X. Lü, Q. Jia, C. Chen, Oxygen content tailored magnetic and electronic properties in cobaltite double perovskite thin films. *Appl. Phys. Lett.* **110**, 093102 (2017).
39. J. R. Sun, H. W. Yeung, H. K. Wong, T. Zhu, B. G. Shen, Effects of vacuum annealing on the transport property of $La_{0.67}Sr_{0.33}MnO_{3-\delta}$ films. *Eur. Phys. J. B* **35**, 481–491 (2003).
40. S. Picozzi, C. Ma, Z. Yang, R. Bertacco, M. Cantoni, A. Cattoni, D. Petti, S. Brivio, F. Ciccacci, Oxygen vacancies and induced changes in the electronic and magnetic structures of $La_{0.67}Sr_{0.33}MnO_3$: A combined ab initio and photoemission study. *Phys. Rev. B* **75**, 094418 (2007).
41. Z. Liao, F. Li, P. Gao, L. Li, J. Guo, X. Pan, R. Jin, E. W. Plummer, J. Zhang, Origin of the metal-insulator transition in ultrathin films of $La_{2/3}Sr_{1/3}MnO_3$. *Phys. Rev. B* **92**, 125123 (2015).
42. D. V. Karpinsky, I. O. Troyanchuk, L. S. Lobanovsky, A. N. Chobot, C. Ritter, V. Efimov, V. Sikolenko, A. L. Kholkin, Magnetic and structural phase transition in $La_{0.5}Sr_{0.5}CoO_{3-\delta}$ ($0 \leq \delta \leq 0.3$) cobaltites. *J. Phys. Condens. Matter* **25**, 316004 (2013).
43. Z. Q. Liu, W. M. Lü, X. Wang, Z. Huang, A. Annadi, S. W. Zeng, T. Venkatesan, Ariando, Magnetic-field induced resistivity minimum with in-plane linear magnetoresistance of the Fermi liquid in $SrTiO_{3-x}$ single crystals. *Phys. Rev. B* **85**, 155114 (2012).
44. A. David, Y. Tian, P. Yang, X. Gao, W. Lin, A. B. Shah, J.-M. Zuo, W. Prellier, T. Wu, Colossal positive magnetoresistance in surface-passivated oxygen-deficient strontium titanite. *Sci. Rep.* **5**, 10255 (2015).
45. R. Scherwitzl, S. Gariglio, M. Gabay, P. Zubko, M. Gibert, J.-M. Triscone, Metal-insulator transition in ultrathin $LaNiO_3$ films. *Phys. Rev. Lett.* **106**, 246403 (2011).
46. T. Ozaki, H. Kino, Efficient projector expansion for the ab initio LCAO method. *Phys. Rev. B* **72**, 045121 (2005).
47. J. P. Perdew, K. Burke, M. Ernzerhof, Generalized gradient approximation made simple. *Phys. Rev. Lett.* **77**, 3865–3868 (1996).
48. S. Thirupathaiah, R. Jha, B. Pal, J. S. Matias, P. Kumar Das, P. K. Sivakumar, I. Vobornik, N. C. Plumb, M. Shi, R. A. Ribeiro, D. D. Sarma, $MoTe_2$: An uncompensated semimetal with extremely large magnetoresistance. *Phys. Rev. B* **95**, 241105 (2017).
49. V. N. Singh, P. Majumdar, Antisite domains in double perovskite ferromagnets: Impact on magnetotransport and half-metallicity. *EPL* **94**, 47004 (2011).
50. D. Sánchez, M. García-Hernández, N. Auth, G. Jakob, Structural, magnetic, and transport properties of high-quality epitaxial Sr_2FeMoO_6 thin films prepared by pulsed laser deposition. *J. Appl. Phys.* **96**, 2736–2742 (2004).
51. A. Gupta, X. W. Li, G. Xiao, Magnetic and transport properties of epitaxial and polycrystalline chromium dioxide thin films (invited). *J. Appl. Phys.* **87**, 6073–6078 (2000).
52. V. N. Antonov, L. V. Bekenov, Electronic structure and x-ray magnetic circular dichroism in $A_2CrB'O_6$ (A = Ca, Sr; B′ = W, Re, and Os) oxides. *Low Temp. Phys.* **43**, 578–589 (2017).
53. M. A. Cortés-Jácome, C. Angeles-Chavez, E. López-Salinas, J. Navarrete, P. Toribio, J. A. Toledo, Migration and oxidation of tungsten, species at the origin of acidity and catalytic activity on WO_3-ZrO_2 catalysts. *Appl. Catal. A* **318**, 178–189 (2007).
54. M. Rutkowski, A. J. Hauser, F. Y. Yang, R. Ricciardo, T. Meyer, P. M. Woodward, A. Holcombe, P. A. Morris, L. J. Brillson, X-ray photoemission spectroscopy of Sr_2FeMoO_6 film stoichiometry and valence state. *J. Vac. Sci. Technol. A* **28**, 1240–1244 (2010).
55. H.-T. Jeng, G. Y. Guo, First-principles investigations of orbital magnetic moments and electronic structures of the double perovskites Sr_2FeMoO_6, Sr_2FeReO_6, and Sr_2CrWO_6. *Phys. Rev. B* **67**, 094438 (2003).

Acknowledgments: We would like to acknowledge NSRL (Hefei) and High Magnetic Field Laboratory (Hefei) for providing the beam time from station BL12B-a and the PPMS-16 measurements, respectively. **Funding:** This work was supported by the 973 Program (2015CB921203), the National Natural Science Foundation of China (U1432112, 51672125, and 11674156), and "Dengfeng B" project of Nanjing University. **Author contributions:** S.-T.Z. conceived the idea and designed the experiments. J. Zhang and W.-J.J. prepared the samples. J. Zhang, W.-J.J., J.X., and X.-Y.G. performed the measurements. J. Zhou carried out the first-principles calculations. All authors contributed to the discussions. J. Zhou and S.-T.Z. wrote the manuscript with revisions from other authors. S.-T.Z. and J. Zhou claim responsibility for all of the figures. **Competing interests:** The authors declare that they have no competing interests. **Data and materials availability:** All data needed to evaluate the conclusions in the paper are present in the paper and/or the Supplementary Materials. Additional data related to this paper can be requested from the authors.

Submitted 5 May 2017
Accepted 16 October 2017
Published 3 November 2017
10.1126/sciadv.1701473

Citation: J. Zhang, W.-J. Ji, J. Xu, X.-Y. Geng, J. Zhou, Z.-B. Gu, S.-H. Yao, S.-T. Zhang, Giant positive magnetoresistance in half-metallic double-perovskite Sr_2CrWO_6 thin films. *Sci. Adv.* **3**, e1701473 (2017).